Single-photon switching in a Floquet waveguide-QED system
with time-modulated coupling constants

Haozhen Li [1,2] Zerong Li,[1] Ran Zeng,[1,*] Miao Hu,[1,†] Mengmeng Xu,[1] Xuefang Zhou,[1]
Xiuwen Xia [3] Jingping Xu,[2,‡] and Yaping Yang[2]

[1]*School of Communication Engineering, Hangzhou Dianzi University, Hangzhou 310018, China*
[2]*Key Laboratory of Advanced Micro-Structured Materials of Ministry of Education, School of Physics Science and Engineering,*
Tongji University, Shanghai 200092, China
[3]*Institute of Atomic and Molecular Physics and Functional Materials, School of Mathematics and Physics,*
Jinggangshan University, Ji'an, 343009, China

The dynamical control of single-photon scattering in a one-dimensional waveguide coupled to a Floquet atom-cavity system with time-modulated coupling constants is investigated. The analytical expressions for determining the scattering properties are obtained by using an effective Floquet Hamiltonian in real space. The photon transport is extremely sensitive to the time-modulated atom-cavity coupling strengths. Two cases, i.e., the effective Floquet Hamiltonian either includes or excludes a static coupling term, are discussed in detail. The results show that, with such Floquet atom-cavity configuration, an active photonic switch with nearly ideal switching contrast could be implemented. The transmission of the waveguide photons with different frequencies can dynamically be switched on or off via adjusting the modulated amplitude or relative modulated phase no matter whether the static coupling between the atom and the two cavity modes is considered or not. The application of the dynamic modulated atom-cavity coupling strengths instead of a purely static one makes our photonic switch more tunable. These results are expected to be applicable in quantum information processing and in active quantum device design involving dynamical modulation.

I. INTRODUCTION

Photons are considered as ideal information carriers for optical information processing due to the fast propagation speed and the ability to retain coherence over long distances [1,2]. How to precisely control the photon propagation is requisite for the efficient operation of quantum networks [3]. Waveguide–quantum electrodynamic (waveguide-QED) structure is one of the main physical platforms for controlling photon transport in a one-dimensional waveguide coupled to different quantum emitters [4–6]. The coupled emitter can work as a tunable scatterer, which scatters the photons in the waveguide into either the forward (transmission) mode or the backward (reflection) mode. Recently, a number of waveguide-based photon transport controlling schemes have been proposed [7–19] and have been demonstrated experimentally [20–24]. Most of these works are related to the designs and fabrications of various quantum devices, such as quantum switches or routers [25–37], single-photon isolators [38–42], and quantum frequency converters or frequency combs [43–47], etc., just to name a few as examples.

Quantum switches, which can coherently interconnect different quantum channels on a level of individual quanta,

are one of the key devices in the fields of quantum networks. In this regard, a variety of theoretical and experimental efforts have been devoted to the realization and development of single-photon switches with high switching efficiency [48–62]. These studies show that, in one-dimensional waveguide-QED architectures, the coupled emitter can behave as either a perfect mirror totally reflecting the waveguide photons, or an ideal transparent medium allowing photons to pass through, which can be used for the implementation of a perfect single-photon switch. Typically, quantum emitters with ladder-type, V-type, Λ-type, and four-level atomic configurations can be utilized to perform the switching functions toward the coupled waveguide photons by driving the auxiliary atomic levels with a classical control field [48–53]. Additionally, a photonic switch with an ideal switching contrast can also be achieved based on atom-cavity systems by manipulating either the atom-cavity and cavity-cavity interactions or the waveguide-cavity couplings [26–28,54–57]. However, in a solid-state physical system, the coupling strengths depend strongly on the relative positions between the atom and cavity, cavity and cavity, or waveguide and cavity, which seems difficult to control well because the relative positions and the corresponding system parameters are fixed once the device is configured. Furthermore, most of the previously proposed switching schemes can operate well only for photons with selected frequencies, e.g., resonant photons. Once the frequencies of the incident photons are altered, the switching capabilities will rapidly diminish and

─────────
*ranzeng@hotmail.com
†miao_hu@foxmail.com
‡xx_jj_pp@hotmail.com

even be lost completely, which restricts the applications of the previous single-photon switches in quantum networks. Therefore, how to effectively manipulate the photon transport and then achieve a dynamically modulated photonic switch for photons with different frequencies is highly desirable and vital for practical applications in quantum information processing.

In this paper, we propose a scheme of a dynamically modulated single-photon switch based on a Floquet QED system which consists of two single-mode cavities and a two-level atom. Different from the previous works reviewed above, where all the system parameters are constants, here the atom couples to the two cavity modes with time-modulated coupling strengths. We focus on exploring how to dynamically control the single-photon scattering process by adjusting the modulated parameters introduced into the coupling strengths. Two cases, where the atom interacts with the cavity modes with or without a static coupling term, are considered. It is found that the Floquet atom-cavity system can act as an ideal active photonic switch with nearly perfect switching contrast. The waveguide photons can dynamically be switched on or off via adjusting the modulated amplitude or relative modulated phase of the atom-cavity coupling strengths. Furthermore, the proposed active photonic switch is efficient for photons with different frequencies even far away from the resonant point. These results should be important and meaningful for designing dynamical modulated photonic devices and applications in future quantum network communication.

The rest of the paper is organized as follows. In Sec. II, we introduce the theoretical model of the Floquet waveguide-QED system and derive the analytical expressions for determining the photon transmission probability with a full quantum mechanical method. In Sec. III, we investigate how to dynamically manipulate the single-photon scattering process by controlling the modulated amplitude and relative modulated phase of the atom-cavity coupling strengths, and show how an ideal photonic switch for photons with different frequencies can be achieved. Finally, a conclusion is drawn in Sec. IV.

II. MODEL AND BASIC THEORY

The model under consideration comprises a one-dimensional waveguide, a two-level atom, and two single-mode cavities (named cavity A and cavity B, respectively), as schematically shown in Fig. 1. The two cavity modes are coupled indirectly to each other via the two-level atom. The coupling strengths between the atom and the cavity modes are periodically modulated $g_j(t) = g_0 + \eta \cos(\nu_d t + \phi_j)$, $(j = a, b)$ with η the modulated amplitude, ν_d the modulated frequency, ϕ_j the modulated phase, and g_0 the static coupling strength. In addition, the waveguide is side coupled to cavity A at the position $x = 0$ with coupling strength V. The total Hamiltonian of the compound system can be written as

$$H = H_c + H_w + H_a + H_{wc} + H_{ca}, \tag{1}$$

where H_c, H_w, and H_a are the free Hamiltonian of the two cavity modes, the waveguide photons, and the atom, respectively. H_{wc} describes the interaction between the waveguide and the
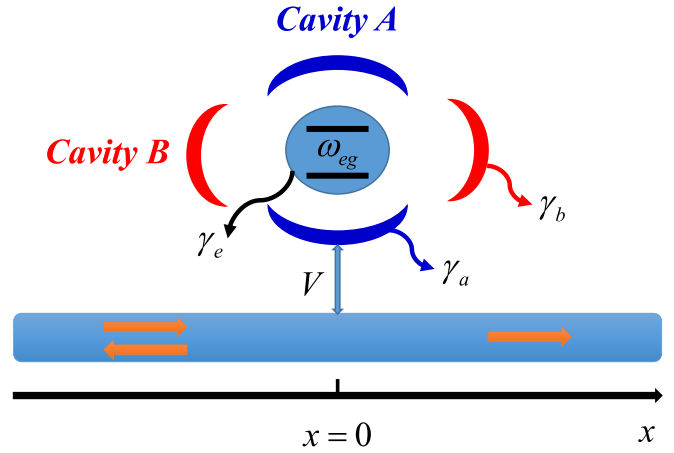

FIG. 1. Schematic diagram of a single-photon scattering in a one-dimensional waveguide side coupled to a Floquet quantum system at $x = 0$ with coupling strength V. The Floquet quantum structure contains a two-level atom (with transition frequency ω_{eg}) and two single-mode cavities (named cavity A and cavity B), wherein the two cavity modes couple to the atom with a time-modulated coupling strength. $\gamma_{a,b}$ and γ_e denote the decay rates of the cavity modes and the atom, respectively.

cavity mode. Finally, H_{ca} refers to the interaction between the atom and the cavity modes.

The Hamiltonian H_c of the two free cavities reads as

$$H_c = \left(\omega_a - i\frac{\gamma_a}{2}\right)a^\dagger a + \left(\omega_b - i\frac{\gamma_b}{2}\right)b^\dagger b, \tag{2}$$

where $a^\dagger$ ($b^\dagger$) and a (b) denote the bosonic creation and annihilation operators of the cavity mode A (B), respectively. ω_j and γ_j are the eigenfrequencies of the cavity modes and their corresponding decay rates.

The free photonic Hamiltonian H_w in real space is given by

$$H_w = i\upsilon_g \int dx c_L^\dagger \frac{\partial}{\partial x} c_L(x) - i\upsilon_g \int dx c_R^\dagger \frac{\partial}{\partial x} c_R(x), \tag{3}$$

where $c_R^\dagger(x)$ [$c_R(x)$] denotes creating (annihilating) a right-moving photon and $c_L^\dagger(x)$ [$c_L(x)$] denotes creating (annihilating) a left-moving photon at the position x in the one-dimensional waveguide. υ_g is the group velocity of a photon in the waveguide. The Hamiltonian for the free atom is

$$H_a = \left(\omega_e - i\frac{\gamma_e}{2}\right)\sigma_{ee} + \omega_g \sigma_{gg}, \tag{4}$$

where ω_e (ω_g) is the eigenfrequency of the excited (ground) state $|e\rangle$ ($|g\rangle$), γ_e is the energy loss rate from the atom to the free space, and $\sigma_{ee} = |e\rangle\langle e|$, $\sigma_{gg} = |g\rangle\langle g|$. The interaction Hamiltonian H_{wc} between the waveguide and the cavity mode reads

$$H_{wc} = V \int dx \delta(x)(c_R^\dagger + c_L^\dagger)a + \text{H.c.}, \tag{5}$$

where H.c. denotes the Hermitian conjugate. H_{ca} takes the form

$$H_{ca} = g_a(t)a^\dagger \sigma_{ge} + g_b(t)b^\dagger \sigma_{ge} + \text{H.c.}, \tag{6}$$

where $\sigma_{eg} = |e\rangle\langle g|$ ($\sigma_{ge} = |g\rangle\langle e|$) is the atomic raising (lowering) ladder operator. According to the Floquet theory [63], we assume the separation between the Floquet sidebands is large enough to make all the high-order frequency components far off-resonant, e.g., $\nu_d \gg g_0$, η, and δ (δ is the frequency detuning between the atom and the cavity modes, which has been assumed to be zero in the following discussion), so the perturbation theory can be applied. The effective Floquet Hamiltonian between the atom and the two cavity modes can be obtained by the standard second-order perturbation as [64–67] (see the Appendix)

$$H_{ca}^{\text{eff}} = g_0(a^\dagger \sigma_{ge} + \sigma_{eg}a) + g_0(b^\dagger \sigma_{ge} + \sigma_{eg}b)$$
$$+ iJ_{\text{eff}}(\sigma_{ee} - \sigma_{gg})(b^\dagger a - a^\dagger b), \quad (7)$$

where $J_{\text{eff}} = \eta^2 \sin(\phi_a - \phi_b)/2\nu_d$ is the effective coupling strength between the two cavity modes, which arises from the time modulation and its value depends strongly on the modulated amplitude, modulated frequency, and the relative modulated phase.

It is worth noting that the effective interaction between the two cavity modes is also related to the atomic state σ_z. It has been shown in [68] that the atomic state σ_z plays two key roles in manipulating the photon transmission in a closed loop formed by three time-modulated cavities: (i) The probabilities of the photon transmission are proportional to the populations of the atom in the states $|e\rangle$ and $|g\rangle$; (ii) photons in one cavity can be transferred to the other two cavities in two opposite directions depending on the atomic states σ_z due to the fact that the complex coupling coefficients between the three cavities introduce an effective magnetic field in the closed loop, which breaks the time-reversal symmetry. However, in the present case (where only two cavities are considered), the closed loop is broken, and the directional photon moving disappears. Consequently, the main contribution of the atomic states σ_z here is to manipulate the photon transmission probabilities, which can be equivalently achieved by adjusting the modulating parameters, e.g., $\Delta\phi = \phi_a - \phi_b$.

Furthermore, we would like to point out that other than modulating the coupling strengths between the atom and the cavity modes, a similar effective Hamiltonian as shown in Eq. (7) can also be obtained by alternatively modulating the cavity frequencies with $\nu_c(t) = \nu + \Delta \sin(\nu_d t + \phi_c)$, $c = a, b$ (see the Appendix).

According to Eq. (7), the Hamiltonian in Eq. (1) of the whole system becomes

$$H_{\text{eff}} = H_c + H_w + H_a + H_{wc} + H_{ca}^{\text{eff}}. \quad (8)$$

Suppose that, at the initial time, the two-level atom was in the ground state and the cavities were empty. Thus, the scattering eigenstate for the Hamiltonian H_{eff} can be expressed as

$$|\Psi\rangle = \int dx \phi_r(x) c_R^\dagger(x)|\upsilon\rangle + \int dx \phi_l(x) c_L^\dagger(x)|\upsilon\rangle$$
$$+ \mu_a a^\dagger|\upsilon\rangle + \mu_b b^\dagger|\upsilon\rangle + \mu_e \sigma_{eg}|\upsilon\rangle, \quad (9)$$

where $\phi_r(x)$ [$\phi_l(x)$] denotes the probability amplitude of the right- (left-) moving photon in the waveguide. μ_a, μ_b, and μ_e are the excitation amplitudes of cavity A, cavity B, and the atom, respectively. $|\upsilon\rangle$ is the vacuum state, which represents

no photon in the waveguide and cavities, and the atom in ground state $|g\rangle$.

From the eigenvalue equation $H_{\text{eff}}|\Psi\rangle = (\omega + \omega_g)|\Psi\rangle$, five coupled linear differential equations can be obtained:

$$-i\upsilon_g \frac{\partial}{\partial x}\phi_r(x) + V\delta(x)\mu_a = \omega\phi_r(x), \quad (10)$$

$$i\upsilon_g \frac{\partial}{\partial x}\phi_l(x) + V\delta(x)\mu_a = \omega\phi_l(x), \quad (11)$$

$$V\phi_r(0) + V\phi_l(0) + g_0\mu_e + iJ_{\text{eff}}\mu_b = \left(\omega - \omega_a + i\frac{\gamma_a}{2}\right)\mu_a, \quad (12)$$

$$g_0\mu_e - iJ_{\text{eff}}\mu_a = \left(\omega - \omega_b + i\frac{\gamma_b}{2}\right)\mu_b, \quad (13)$$

$$g_0\mu_a + g_0\mu_b = \left(\omega - \omega_{eg} + i\frac{\gamma_e}{2}\right)\mu_e, \quad (14)$$

where $\omega_{eg} = \omega_e - \omega_g$ is the transition frequency of the two-level atom. For photons incident from the left, the amplitudes $\phi_r(x)$ and $\phi_l(x)$ take the form

$$\phi_r(x) = e^{ikx}[s(-x) + ts(x)],$$
$$\phi_l(x) = e^{-ikx}rs(-x), \quad (15)$$

where $k = \omega/\upsilon_g$ and $s(x)$ is the step function with $s(0) = 1/2$. t (r) denotes the photon transmission (reflection) amplitude in the waveguide. Substituting Eq. (15) into Eqs. (10)–(14), one can obtain

$$t = \frac{J_{\text{eff}}^2 k_e + g_0^2(k_a + k_b) - k_a k_b k_e}{J_{\text{eff}}^2 k_e + g_0^2(k_a + k_b + i\Gamma) - k_b k_e(k_a + i\Gamma)}, \quad (16)$$

$$r = \frac{-i\Gamma(g_0^2 - k_b k_e)}{J_{\text{eff}}^2 k_e + g_0^2(k_a + k_b + i\Gamma) - k_b k_e(k_a + i\Gamma)}, \quad (17)$$

where $\Gamma = V^2/\upsilon_g$ denotes the coupling loss between cavity A and the waveguide. $k_{j=a,b} = \Delta_j + i\gamma_j/2$ and $k_e = \Delta_{eg} + i\gamma_e/2$ with $\Delta_j = \omega - \omega_j$ ($\Delta_{eg} = \omega - \omega_{eg}$) the frequency detuning between the waveguide photons and the cavity modes (atom). In the following discussions, without loss of generality, we assume that $\omega_a = \omega_b = \omega_{eg} \equiv \omega_c$, corresponding to $\Delta_a = \Delta_b = \Delta_{eg} \equiv \Delta$.

Furthermore, in order to quantitatively analyze the single-photon scattering properties in the waveguide, we introduce the dimensionless quantities $T = |t|^2$ and $R = |r|^2$ for describing the transmission and reflection probabilities, which satisfies the conservation condition $T + R = 1$ when the dissipations of the atom and the cavities to other modes are ignored. However, in practice, the influence of the intrinsic dissipative processes of the system should be taken into account, which makes the sum of $T + R$ slightly smaller than 1.

III. RESULTS AND DISCUSSIONS

In this section, we investigate the properties of the single-photon scattering for two possible cases (namely, the atom interacts with the two cavity modes with or without a static coupling term) based on the analytical expressions as shown in Eqs. (16) and (17). We focus on exploring how the photon scattering process is controlled by the time modulation. In detail, we analyze the influences of the time-modulated system parameters, including the modulated amplitude η and the
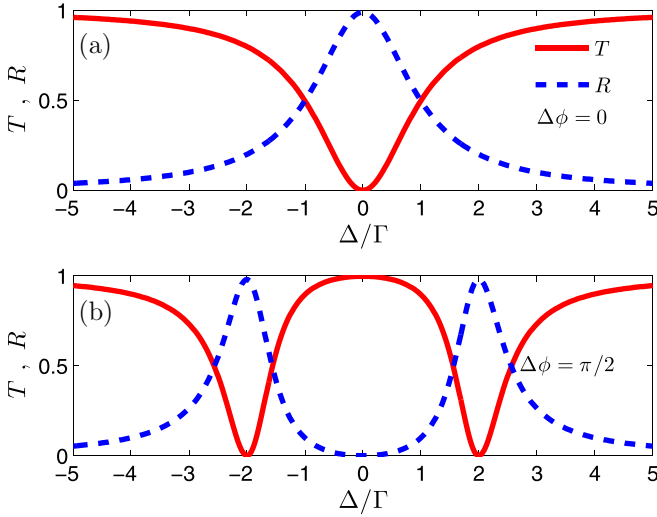
FIG. 2. The transmission and reflection probabilities as a function of the frequency detuning Δ/Γ for two different values of the relative modulated phases: $\Delta\phi = 0$ in (a) and $\Delta\phi = \pi/2$ in (b). The other common parameters are $\eta = 200\Gamma$, $\nu_d = 50\eta$, $g_0 = 0$, and $\gamma_e = \gamma_a = \gamma_b = 0.01\Gamma$, respectively.

relative modulated phase $\Delta\phi = \phi_a - \phi_b$ of the atom-cavity coupling strengths, on the photon transport, and show how a dynamically modulated photonic switch with nearly ideal switching contrast could be implemented.

A. Scattering spectra of a single photon without static atom-cavity coupling $g_0 = 0$

First, we study how the transmission and reflection spectra vary with the relative modulated phase $\Delta\phi$ for a given modulated amplitude $\eta = 200\Gamma$ and show how a phase-sensitive single-photon switch with nearly ideal switching contrast could be implemented in the absence of static coupling (i.e., $g_0 = 0$). In Fig. 2, we plot the photon transmission and reflection probabilities (T and R) as a function of the frequency detuning Δ/Γ for two different cases: namely, the two coupling strengths g_a and g_b are modulated in phase (i.e., $\Delta\phi = 0$), or out of phase (i.e., $\Delta\phi \neq 0$). For the case of $\Delta\phi = 0$, the reflection (transmission) spectrum displays a Lorentzian (inverted Lorentzian) line shape with $R \approx 1$ ($T \approx 0$) at the resonance point [see the blue dashed (red solid) line in Fig. 2(a)], which implies that the resonantly incident photon is nearly perfectly reflected and the transmission vanishes. This can be explained from the effective interaction Hamiltonian H_{ca}^{eff} shown in Eq. (7). Under the conditions $g_0 = 0$ and $\Delta\phi = 0$ [corresponding to $J_{\mathrm{eff}} = \eta^2 \sin(\phi_a - \phi_b)/2\nu_d = 0$], H_{ca}^{eff} becomes zero; the effective atom-cavity and cavity-cavity interactions disappear. This means that both the atom and cavity B are decoupled from cavity A, and the whole considered system is degenerated into a one-dimensional waveguide side coupled by a single-mode cavity. It is well known that, in this case, the single-mode cavity can act as a perfect mirror due to the destructive interference between the incident photons and the reemitted one, which leads to the cancellation of the photon transmission.
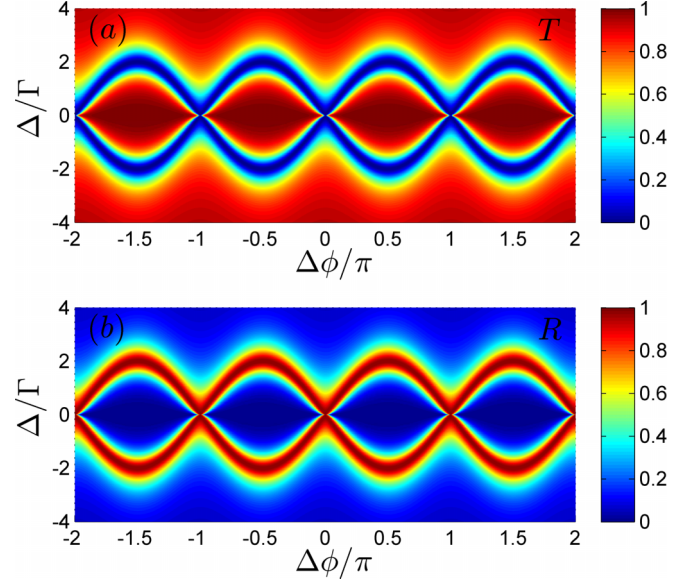

FIG. 3. The contour map of the transmission (a) and reflection (b) spectrum as a function of both Δ/Γ and $\Delta\phi$. Other common parameters are the same as those shown in Fig. 2.

For the case of $\Delta\phi \neq 0$ (i.e., $\Delta\phi = \pi/2$), the transmission line shape transits from an inverted Lorentzian profile to the so-called coupled-resonator-induced transparency profile, quantified by a transparent resonance peak and two symmetric sideband dips [see the red solid line in Fig. 2(b)]. The reason is that the effective coupling strength between the two cavity modes becomes nonzero (i.e., $J_{\mathrm{eff}} = 2\Gamma$) when $\Delta\phi = \pi/2$, which leads to the normal mode splitting in the present double-cavity system. Consequently, a resonantly incident single photon with $\Delta = 0$ is far detuned from the frequencies of the two normal modes, resulting in the single photon in the waveguide transmitting completely ($T \approx 1$) without reflecting ($R \approx 0$). Thus, from Fig. 2, one can come to a conclusion that the considered Floquet atom-cavity system can behave as a nearly perfect active photonic switch based on the relative modulated phase. When the two coupling strengths g_a and g_b are modulated in phase, $\Delta\phi = 0$, the transmission of a resonantly incident waveguide photon almost vanishes, which means that the device is switched off. On the contrary, when g_a and g_b are modulated out of phase, $\Delta\phi \neq 0$, the transmission of the incident photon is switched on with $T \approx 1$ at the resonance point.

In order to illustrate how to control the switching probability through varying the relative modulated phase in a more general case, the variations of T and R versus both Δ/Γ and $\Delta\phi$ for a selected modulated amplitude $\eta = 200\Gamma$ are plotted in Figs. 3(a) and 3(b), respectively. It is shown that, for the resonantly incident single photon with $\Delta = 0$, the device persists in switching on with $T \approx 1$ except at the in-phase points, i.e., $\Delta\phi = n\pi$, $n = 0, \pm1, \pm2, \cdots$, which is consistent with that shown in Fig. 2. Furthermore, it can be found that the switching window and the optimal switching points are phase sensitive. The transmission or reflection bandwidth of the photons scattered by the Floquet atom-cavity structure can be dynamically modulated by controlling the relative modulated phase. For instance, increasing $\Delta\phi$ from
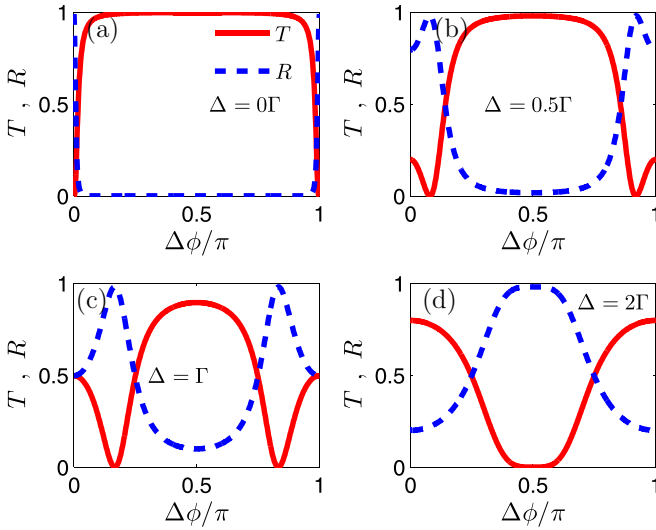
FIG. 4. The transmission and reflection probabilities as a function of the relative modulated phase for different photon frequencies with $\Delta/\Gamma = 0$, 0.5, 1, 2 in (a–d), respectively. Other common parameters are the same as those shown in Fig. 2.

FIG. 5. The contour map of the transmission (a) and reflection (b) spectrum as the function of both Δ/Γ and η/Γ. Other common parameters are the same as those shown in Fig. 2, except that $\Delta\phi = \pi/2$.

0 to $\pi/2$, the on-resonance transmission peak becomes flat [see the bright red zone in Fig. 3(a)] and the two sideband dips shift toward both sides [see the two bright blue zones in Fig. 3(a)].

The physical mechanism of this phase-dependent single-photon switch can further be explained in the normal mode picture [69]. As is well known, the interactions between two cavities and an atom will result in the generation of a pair of standing wave modes A and B, which are the superposition of the two cavity modes, i.e., $A = (a + b)/\sqrt{2}$ and $B = (a - b)/\sqrt{2}$. As discussed above, under the condition $g_0 = 0$ and $\Delta\phi \neq 0$, the time-modulated atom-cavity system is equivalent to two coupled cavities. Thus, in the new normal mode representation, the effective Hamiltonian of the whole system can be reduced to the form $H_{\text{eff}} \rightarrow \hbar(\omega_c + J_{\text{eff}})A^{\dagger}A + \hbar(\omega_c - J_{\text{eff}})B^{\dagger}B$ with ω_c the frequency of the cavity modes. One can find that the resonant frequencies of the normal modes A and B are modified as $\omega_A = \omega_c + J_{\text{eff}}$ and $\omega_B = \omega_c - J_{\text{eff}}$, respectively. Thus, an incident photon on resonance with the normal mode A or B will be nearly completely reflected without transmission [which corresponds to the reflection peaks or transmission dips in Fig. 2(b)] due to the destructive interference. Moreover, both ω_A and ω_B are closely related to the phase difference $\Delta\phi = \phi_a - \phi_b$ due to the fact that $J_{eff} = \eta^2 \sin(\phi_a - \phi_b)/2\nu_d$. This suggests that, for given η and ν_d, one can tune the frequency values where perfect switching is attained by altering the relative modulated phase between the two atom-cavity couplings. This also implies that a dynamically modulated high-efficiency photonic switch for photons with different frequencies can be realized.

To show this clearly, the transmission spectrum T and the reflection spectrum R varying with $\Delta\phi$ for an incident single photon with a series of selected frequencies, i.e., $\Delta/\Gamma = 0$, 0.5, 1, 2, are plotted in Fig. 4. It can be seen from Figs. 4(a) and 4(b) that when the incident single photon has frequencies around the resonant point, the photon can be
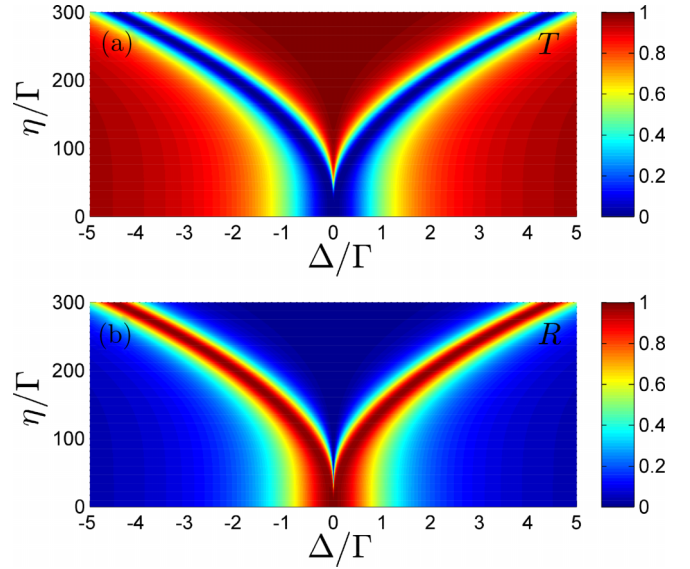
tuned from nearly completely reflection (i.e., $R \approx 1$, $T \approx 0$) to totally transmission (i.e., $R \approx 0$, $T \approx 1$) depending on $\Delta\phi$, and vice versa. This means that a nearly ideal photonic switch for photons with different frequencies can be implemented by properly designing and adjusting the relative modulated phase. However, we would like to point out that the reflected photons cannot be tuned to transmit with a perfect transmission probability (i.e., $T < 1$) as the detuning $|\Delta|$ becomes larger [see the red solid line in Figs. 4(c) and 4(d)], which implies that when the selected frequencies of the incident photons are far away from the resonant point, the efficiency of the phase-sensitive single-photon switch decreases. In general, this shortcoming could be overcome by further adjusting the modulated amplitude η.

Below, we demonstrate how to control the single-photon scattering through varying the modulated amplitude η for a given $\Delta\phi = \pi/2$. The transmission and reflection probability versus both the frequency detuning Δ/Γ and the modulated amplitude η are plotted in Figs. 5(a) and 5(b), respectively. It is obvious from Fig. 5 that the transmission and reflection spectrum are closely related to the modulated amplitude. When η is very small, T and R remain nearly unchanged with the increase of η, i.e., $T \approx 0$ and $R \approx 1$ at $\Delta = 0$, which means that both the transmission and reflection probabilities are insensitive to the modulated amplitude. This is because, when η is extremely weak, the composite Floquet atom-cavity system is reduced to a single-mode cavity, which agrees well with that discussed in Fig. 2(a). With η gradually increasing, J_{eff} becomes nonzero; the effective coupling between the two cavity modes plays an essential role in the spectral line shapes and gives rise to a splitting of the resonant dip and peak, as shown by the two bright blue and red zones in Figs. 5(a) and 5(b), respectively. The width between the two dips or peaks increases with the increase of η. According to what is discussed in Figs. 3 and 4, this behavior suggests that the op-
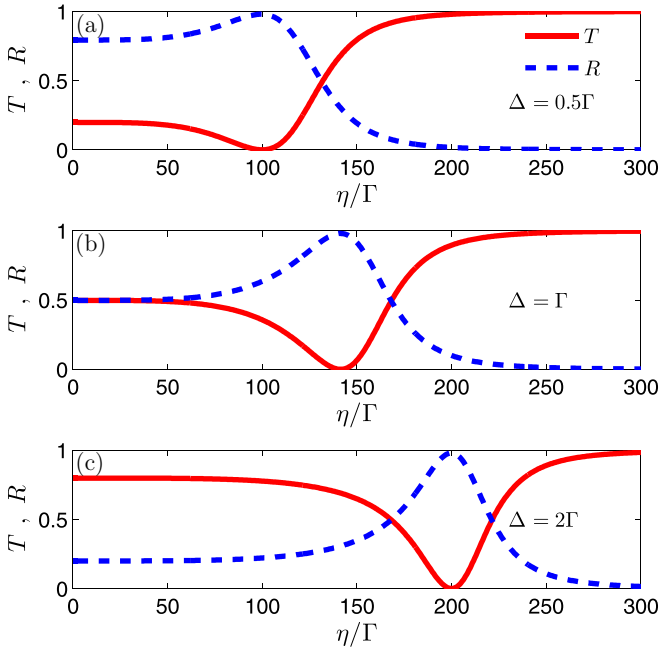
FIG. 6. The transmission and reflection probabilities as a function of the modulated amplitude for different photon frequencies with $\Delta/\Gamma = 0.5$, 1, 2 in (a–c), respectively. Other common parameters are the same as those shown in Fig. 2, except that $\Delta\phi = \pi/2$.
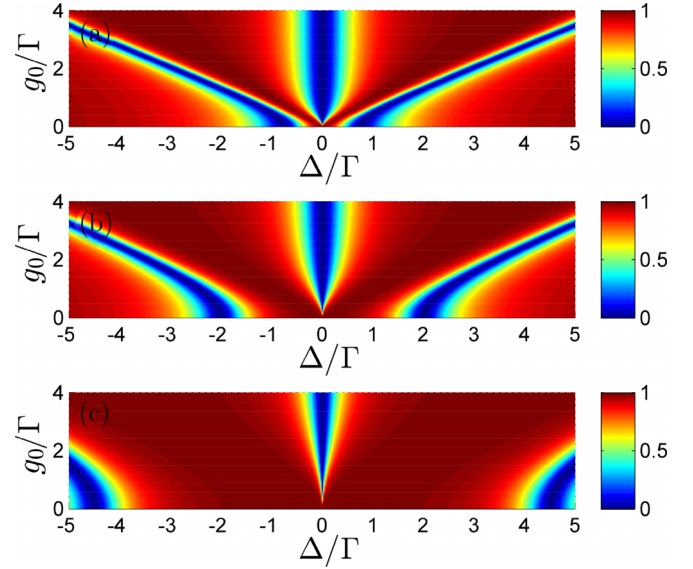

FIG. 7. The contour map of the transmission spectrum as a function of both Δ/Γ and g_0/Γ for a series of modulated parameters, i.e., ($\eta = 200\Gamma$, $\Delta\phi = \pi/8$), ($\eta = 200\Gamma$, $\Delta\phi = \pi/2$), and ($\eta = 300\Gamma$, $\Delta\phi = \pi/2$) in (a–c), respectively. Other common parameters are the same as those shown in Fig. 2.

timal switching point can be further shifted toward both sides depending on η. Consequently, by carefully manipulating the modulated amplitude, the proposed single-photon switch is also efficient for the incident photons with frequencies far away from the resonant point.

For further insight into this remarkable feature, we specially demonstrate how to control the switching probabilities T and R by the modulated amplitude η for the case of a series of selected frequencies, i.e., $\Delta/\Gamma = 0.5$, 1, 2. It can be seen from Fig. 6 that the transmission (reflection) probability of photons with different frequencies can be tuned from $T \approx 0$ ($R \approx 1$) to $T \approx 1$ ($R \approx 0$) by increasing η. This implies that the switching on and off state of the incident photons can be effectively controlled by properly adjusting the modulated amplitude, and a nearly ideal photonic switch for photons with different frequencies far away from the resonant point can be achieved. Furthermore, one can find that, as the photonic frequency detuning $|\Delta|$ increases, a relatively high value of η for the ideal photonic switch is needed. In principle, the proposed dynamically modulated single-photon switch is valid for photons within arbitrary frequency regimes.

B. Scattering spectra of a single photon with static atom-cavity coupling $g_0 \neq 0$

In previous discussions, we mainly focused on how a nearly ideal photonic switch can be realized and be controlled by the time modulations in the absence of the static coupling with $g_0 = 0$. However, physically, the coupling strength between the atom and the cavity modes plays an important role in the photon scattering process. In what follows, the dynamical modulations of such an ideal photonic switch are

further demonstrated by considering the influences of the static coupling with $g_0 \neq 0$.

In Fig. 7, the variations of the transmission probability T versus both Δ/Γ and g_0 with different modulated amplitudes and relative modulated phases are plotted, i.e., ($\eta = 200\Gamma$, $\Delta\phi = \pi/8$), ($\eta = 200\Gamma$, $\Delta\phi = \pi/2$), and ($\eta = 300\Gamma$, $\Delta\phi = \pi/2$) in Figs. 7(a)–7(c), respectively. It can be seen from Fig. 7 that the existence of the static coupling strength modifies the transport behaviors of the waveguide photons. There are two peaks (see the two bright red zones) and three dips (see the three bright blue zones) in the transmission spectrum, which is in sharp contrast to the obtained results shown in Figs. 2 and 3. The underlying physics can be explained as below. By dynamically modulating the coupling strengths between the atom and the cavity modes with $g_0 = 0$, the effective coupling between the two cavity modes splits the resonant transmission dip into two sideband dips, which has been shown in Fig. 2. If the static coupling $g_0 \neq 0$ is taken into account, the transmission peak [denoted by the red solid line in Fig. 2(b)] can be further split into two sideband ones due to the well-known Rabi splitting originating from the interactions between the atom and the cavity modes [70]. As a result, the three transmission dips denoted by the bright blue zones in Fig. 7 correspond to three nondegenerate eigenmodes with frequencies located at $\Delta = 0$ and $\Delta = \pm\sqrt{J_{\text{eff}}^2 + 2g_0^2}$ [with $J_{\text{eff}} = \eta^2 \sin(\phi_a - \phi_b)/2\nu_d$], respectively.

Obviously, the width between different dips (or the width of each transmission peak) is sensitive to both the static coupling strength and the dynamical modulated parameters. Figure 7 shows that, increasing g_0, the two sideband dips shift toward both sides for a pair of selected η and $\Delta\phi$. Comparing Figs. 7(a) and 7(b), for fixed g_0 and η, a similar behavior can be obtained by increasing the relative modulated phase to $\Delta\phi = \pi/2$, and the width can be further broadened by
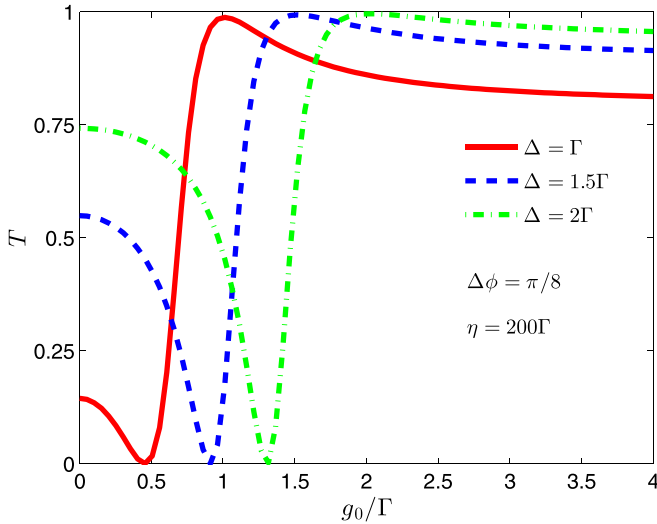
FIG. 8. The transmission probabilities as a function of the static coupling strength g_0/Γ for different photon frequencies with $\Delta/\Gamma = 1, 1.5, 2$. Other common parameters are the same as those shown in Fig. 2, except that $\Delta\phi = \pi/8$.

tuning the modulated amplitude from $\eta = 200\Gamma$ to $\eta = 300\Gamma$ [as shown in Fig. 7(c)].

On the basis of what was discussed in Sec. III A, the existence of transmission peaks (or dips) with neighboring dips (or peaks) in the photon scattering spectra is a key premise for photon switching, and the increased number of the transmission peaks and dips is beneficial for switching photons with different frequencies. Thus, it is clear from Fig. 7 that a dynamically modulated photonic switch for photons with different frequencies far away from the resonant point can still be achieved in the presence of the static coupling with $g_0 \neq 0$. For further insight, the transmission probability versus the static coupling strength and the dynamical modulated parameters are given in Figs. 8 and 9, respectively.
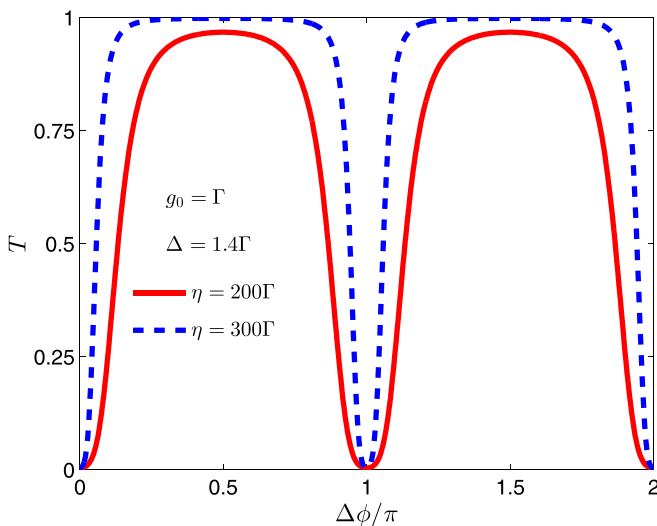

FIG. 9. The transmission probabilities as a function of the relative modulated phase with different modulated amplitudes. Other common parameters are the same as those shown in Fig. 2, except that $g_0 = \Gamma$.

In Fig. 8, we show how a high-efficiency photonic switch for photons with different frequencies, i.e., $\Delta/\Gamma = 1, 1.5, 2$, can be implemented by manipulating the static coupling strength g_0. It can be seen that, for fixed $\eta = 200\Gamma$ and $\Delta\phi = \pi/8$, the static coupling g_0 plays an important role in manipulating the photonic switching. The transmission probability can be tuned from $T \approx 0$ to $T \approx 1$ by increasing g_0, which means that the incident photons can effectively be switched on or off through varying the static coupling strength. This result is similar to that obtained in the previous static atom-cavity systems, where the photonic switch is realized by tuning the atom-cavity interaction strengths from the weak coupling regimes to the strong ones (which might not be easy to realize experimentally). However, we highlight that the proposed switching scheme here can be effectively implemented within the regime $g_0 < \Gamma$ (and even close to zero).

In Fig. 9, we further demonstrate how to achieve the photonic switching by controlling the modulated parameters with a fixed static coupling strength $g_0 = \Gamma$. The results show again that the transmission probability T is a periodic function of the relative modulated phase $\Delta\phi$ in the presence of the static coupling. The single-photon transport in the waveguide can be switched on or off periodically by adjusting the relative modulated phase. Within a period, the photons with a selected frequency, i.e., $\Delta = 1.4\Gamma$, can be tuned from nearly completely reflection to transmission with $T \approx 0.95$; see the red solid line. The switching probability can be further improved to $T \approx 1$ by increasing the modulated amplitude to $\eta = 300\Gamma$ (see the blue dashed line), which implies that an ideal single-photon switch with nearly perfect switching contrast is realized.

C. Physical implementation

In this section, we provide a brief discussion on the experimental feasibility of our scheme under the existing experimental techniques. Different technologies and platforms for physical implementation, realistic parameter values in experiment, and possible experimental errors are addressed, respectively.

Our scheme is composed of two single-mode cavities, a two-level atom, and a one-dimensional waveguide. This system can be achieved in superconducting circuits [71], where the two-level atom can be a superconducting qubit, the cavities can be two superconducting resonators, and the waveguide can be a superconducting transmission line. In our model, a key element is the time-modulated coupling between the atom and the two cavity modes, which can be realized by embedding a superconducting quantum interference device (SQUID) between the qubit and the two resonators [72–74]. The effective coupling between the two resonators can be realized and controlled through tuning the SQUIDs. Thus, if the superconducting transmission line can be effectively connected by the resonator, then the single-photon switch may be demonstrated in the proposed system. Furthermore, this scheme may also be implemented in optomechanical circuits or a photonic-crystal resonator lattice, where the dynamical modulation can be realized by applying an external time periodic driven field via an auxiliary qubit or an intermediate resonator [75,76].

Next, we examine the realistic parameter space for physical implementation of the dynamical single-photon switch in a circuit-QED system. A key requirement for this physical implementation is that the effective coupling strength between the two resonators should be larger than the decoherence rates of the resonators and the qubit, such that a photon can propagate in the time-modulated system before it is damped. Using the parameters presented in the numerical simulation, we can obtain $J_{\text{eff}} = 2\Gamma$. By setting $\Gamma/2\pi \approx 5$ MHz [77], the effective coupling strength $J_{\text{eff}}/2\pi$ is about 10 MHz, which is well above the intrinsic decay rate of the resonators and the qubit, estimated as ≈ 0.05 MHz. We note that the effective coupling strength J_{eff} is proportional to the ratio of η^2/ν_d. As discussed in [78], $\nu_d \approx 5\eta$ is large enough to separate the Floquet bands. Thus, by setting $\eta/2\pi \approx 100$ MHz as a typical coupling constant attainable with modern circuit-QED technologies [79,80], one can also arrive at $J_{\text{eff}}/2\pi \approx 10$ MHz.

Finally, we provide some remarks on the possible experimental errors in the physical implementations. As discussed in [65,81,82], the possible experimental error sources of our scheme may include imperfections in the fabrication of the sample; decoherence; possible inaccuracy in measuring the system parameters, e.g., qubit-resonator coupling strengths; and nonideality of the two modulation parameters (the amplitude η and the frequency ν_d). Among these, the nonideality of the modulation parameters (which are limited by the dynamical range of the hardware tunability) may be one of the main sources of the total error. Fortunately, the hardware tunability may be improved in the near future, and this nonideality error can be significantly reduced by increasing η and ν_d.

IV. CONCLUSION

In conclusion, we have theoretically investigated the single-photon scattering characteristics in a Floquet waveguide-QED system which consists of a one-dimensional waveguide, two single-mode cavities, and a two-level atom. Different from previous works, where all the system parameters are constant, we proposed an effective proposal to control the single-photon scattering process by dynamically modulating the coupling strength between the two-level atom and the cavity modes. The results indicate that the scattering properties of photons along the waveguide can effectively be controlled by the side coupled Floquet atom-cavity system, and an ideal single-photon switch with nearly perfect switching efficiency for photons with different frequencies can be achieved by dynamically manipulating the modulated amplitude and the relative modulated phase, regardless of whether the static coupling between the atom and the two cavity modes is considered or not. The application of a dynamical modulated atom-cavity coupling strength instead of a purely static one makes our photonic switch more tunable, which should be important and meaningful for future quantum network communication.

Furthermore, we would like to note that the proposed dynamical mechanism for controlling single-photon transport is general, which can easily and efficiently be applied to various types of nano- or microscale hybrid quantum systems involving multiple photons and even other neutral polaritons. On the other hand, our proposal might be extended to many-body quantum systems, e.g., photonic resonator lattices, which offers an ideal platform for quantum simulations in high-dimensional topological physics.

APPENDIX: DERIVATION OF EFFECTIVE HAMILTONIAN

In order to obtain the effective Hamiltonian shown in Eq. (7), the Hamiltonian of the considered atom-cavity system can be rewritten as

$$H_S^g = \frac{1}{2}\hbar\omega_{eg}\sigma_z + \sum_{c=a,b} \hbar\omega_{\text{cav}}c^\dagger c + \sum_{c=a,b} [\hbar g_c(t)c^\dagger\sigma_{ge} + \text{H.c.}].$$

(A1)

The first two terms are the Hamiltonians of the atom and the two cavities, respectively. The last term is the interaction between the cavity mode and the atom. ω_{eg} is the atomic transition frequency and ω_{cav} is the cavity frequency. $\sigma_{ge} = |g\rangle\langle e|$ and $\sigma_z = |e\rangle\langle e| - |g\rangle\langle g|$ are the atomic lowering operator and the z-component Pauli matrix, respectively. $c^\dagger$ and c ($c = a, b$) denote the bosonic creation and annihilation operators of the cavity mode. The coupling strengths between cavity c and the atom are periodically modulated $g_c(t) = g_0 + \eta\cos(\nu_d t + \phi_c)$, ($c = a, b$) with η being the modulating amplitude, ν_d the modulating frequency, ϕ_c the modulating phase, and g_0 the static coupling constant. Such time-modulated coupling constants are usually found in Hamiltonians describing the generation of synthetic magnetic fields in superconducting-circuit and photonic resonator lattices [75,81,83].

Assuming $V_0^g = \hbar\omega_{\text{cav}}\sigma_z/2 + \hbar\omega_{\text{cav}}(a^\dagger a + b^\dagger b)$, we can transform the Hamiltonian in Eq. (A1) into a frame rotating with V_0^g,

$$H_I^g = U_0(t)H_S^g U_0^{-1}(t) - V_0^g$$

(A2)

where $U_0(t) = \exp[\int \frac{i}{\hbar}V_0 dt']$ is the unitary evolution operator. Thus, the resultant Hamiltonian reduces to

$$H_I^g = \frac{1}{2}\hbar\delta\sigma_z + \hbar \sum_{c=a,b} [g_c(t)c^\dagger\sigma_{ge} + \text{H.c.}],$$

(A3)

where $\delta = \omega_{eg} - \omega_{\text{cav}}$. By substituting $g_c(t)$ into Eq. (A3), we can expand this Hamiltonian as a sum $H_I^g = H_0^g + H_{\pm 1}^g e^{\pm i\nu_d t}$ with

$$H_0^g = \frac{1}{2}\hbar\delta\sigma_z + \hbar g_0 \sum_{c=a,b} (c^\dagger\sigma_{ge} + \sigma_{eg}c),$$

(A4)

$$H_{\pm 1}^g = \hbar\frac{\eta}{2} \sum_{c=a,b} (c^\dagger\sigma_{ge} + \sigma_{eg}c)\exp(\pm i\phi_c).$$

(A5)

Note that $H^g_{\pm 1}$ are not Hermitian themselves, but H^g_{+1} is the Hermitian conjugate of H^g_{-1}. According to the Floquet theory [63], for the sake of simplicity, we assume the separation between the Floquet sidebands is large enough to make all the high-order frequency component far off resonant, e.g., $\nu_d \gg g_0$, η, and δ, so the perturbation theory can be applied. The effective Hamiltonian can be obtained by standard second-order perturbation as [64–67]

$$H^g_{\mathrm{eff}} = H^g_0 + H^g_{\mathrm{2nd}}, \tag{A6}$$

with

$$
\begin{aligned}
H^g_{\mathrm{2nd}} &= \frac{1}{\hbar \nu_d}\big[H^g_{+1}, H^g_{-1}\big] \\
&= i\hbar J_{\mathrm{eff}}(\sigma_{ee} - \sigma_{gg})(b^\dagger a - a^\dagger b),
\end{aligned}
\tag{A7}
$$

where $J_{\mathrm{eff}} = \frac{\eta^2}{2\nu_d}\sin(\phi_a - \phi_b)$. Combing Eqs. (A4)–(A7) and given $\delta = 0$, we can derive

$$
\begin{aligned}
H^g_{\mathrm{eff}} &= \hbar g_0 \sum_{c=a,b}(c^\dagger \sigma_{ge} + \sigma_{eg}c) \\
&\quad + i\hbar J_{\mathrm{eff}}(\sigma_{ee} - \sigma_{gg})(b^\dagger a - a^\dagger b),
\end{aligned}
\tag{A8}
$$

which is the desired effective Hamiltonian shown in Eq. (7).

It is worth pointing out that, other than modulating the coupling strengths between the atom and the cavity modes, such effective Hamiltonian can also be obtained by alternatively modulating the cavity frequencies $\nu_c(t) = \nu + \Delta \sin(\nu_d t + \phi_c)$, $c = a, b$ with Δ being the modulating amplitude, ν_d the modulating frequency, ϕ_c the modulating phase, and ν the cavity idle frequency.

Under the rotating-wave approximation, the Hamiltonian of the system can now be written as

$$H^{\mathrm{cav}}_S = \frac{1}{2}\hbar \omega_{eg}\sigma_z + \sum_{c=a,b}\hbar \nu_c(t)c^\dagger c + \sum_{c=a,b}\hbar g_\nu(\sigma_{eg}c + \mathrm{H.c.}). \tag{A9}$$

Along a similar line as above, we can transform the Hamiltonian H^{cav}_S into a frame rotating with $V^{\mathrm{cav}}_0 = \hbar \nu \sigma_z/2 + \hbar \nu(a^\dagger a + b^\dagger b)$; then the Hamiltonian has the following form:

$$H^{\mathrm{cav}}_I = \frac{1}{2}\hbar \delta_{eg}\sigma_z + \sum_{c=a,b}\hbar g_\nu(\sigma_{eg}c e^{if\cos(\nu_d t + \phi_c)} + \mathrm{H.c.}). \tag{A10}$$

Here $\delta_{eg} = \omega_{eg} - \nu$ is the detuning between the atom and cavity idle frequency; $f = \Delta/\nu_d$ is the cavity modulating parameter. Using the relationship $e^{if\cos(\nu_d t + \phi_c)} = \sum_{n=-\infty}^{\infty} i^n J_n(f)e^{in(\nu_d t + \phi_c)}$, where $J_n(f)$ is the nth − order Bessel's function of the first kind, we expand the interaction Hamiltonian into a Fourier series,

$$H^{\mathrm{cav}}_I = H^{\mathrm{cav}}_0 + \sum_{n\neq 0}^{\pm\infty} H^{\mathrm{cav}}_n e^{in\nu_d t}, \tag{A11}$$

with

$$
\begin{aligned}
H^{\mathrm{cav}}_0 &= \hbar \delta_{eg}\sigma_z/2 + \hbar g_\nu J_0(f)\sum_{c=a,b}(\sigma_{eg}c + \mathrm{H.c.}), \\
H^{\mathrm{cav}}_n &= \hbar g_\nu i^n J_n(f)\sum_{c=a,b}[\sigma_{eg}c + (-1)^n c^\dagger \sigma_{ge}]e^{in\phi_c}.
\end{aligned}
\tag{A12}
$$

H^{cav}_n is the Hermitian conjugate of H^{cav}_{-n}. Here n should be integers running from negative infinity to positive infinity and $n \neq 0$. Under the condition $\nu_d \gg \sqrt{N}g_\nu$ and δ_{eg}, with N being the total excitation number of the atom and photons, the perturbation theory is valid. The effective Hamiltonian can be obtained by standard second-order perturbation as [63–67]

$$H^{\mathrm{cav}}_{\mathrm{eff}} = H^{\mathrm{cav}}_0 + H^{\mathrm{cav}}_{\mathrm{2nd}}, \tag{A13}$$

with

$$
\begin{aligned}
H^{\mathrm{cav}}_{\mathrm{2nd}} &= \sum_{n=1}^{\infty}\frac{1}{\hbar n\nu_d}[H_n, H_{-n}] \\
&= i\hbar\kappa\sigma_z(b^\dagger a - a^\dagger b),
\end{aligned}
\tag{A14}
$$

where $\kappa = g_\nu^2 \beta(f)/\nu_d$ and $\beta(f) = \sum_{n=1}^{\infty} 2J_n^2(f)\sin[n(\phi_a - \phi_b)]/n$. Thus, given $\delta_{eg} = 0$, a similar effective Hamiltonian can be obtained as

$$H^{\mathrm{cav}}_{\mathrm{eff}} = \hbar g_\nu J_0(f)\sum_{c=a,b}(\sigma_{eg}c + \mathrm{H.c.}) + i\hbar\kappa\sigma_z(b^\dagger a - a^\dagger b). \tag{A15}$$

[1] T. E. Northup and R. Blatt, Quantum information transfer using photons, Nat. Photonics **8**, 356 (2014).

[2] J. L. O'Brien, A. Furusawa, and J. Vučković, Photonic quantum technologies, Nat. Photonics **3**, 687 (2009).

[3] H. J. Kimble, The quantum internet, Nature (London) **453**, 1023 (2008).

[4] Z. Liao, X. Zeng, H. Nha, and M. S. Zubairy, Photon transport in a one-dimensional nanophotonic waveguide QED system, Phys. Scr. **91**, 063004 (2016).

[5] X. Gu, A. F. Kockum, A. Miranowicz, Y.-x. Liu, and F. Nori, Microwave photonics with superconducting quantum circuits, Phys. Rep. **718**, 1 (2017).

[6] D. Roy, C. M. Wilson, and O. Firstenberg, Colloquium: Strongly interacting photons in one-dimensional continuum, Rev. Mod. Phys. **89**, 021001 (2017).

[7] M.-T. Cheng, X.-S. Ma, J.-Y. Zhang, and B. Wang, Single photon transport in two waveguides chirally coupled by a quantum emitter, Opt. Express **24**, 19988 (2016).

[8] N. Liu, X. Wang, X. Wang, X.-S. Ma, and M.-T. Cheng, Tunable single photon nonreciprocal scattering based on giant atom-waveguide chiral couplings, Opt. Express **30**, 23428 (2022).

[9] J.-T. Shen and S. Fan, Coherent photon transport from spontaneous emission in one-dimensional waveguides, Opt. Lett. **30**, 2001 (2005).

[10] L. Yuan, S. Xu, and S. Fan, Achieving nonreciprocal unidirectional single-photon quantum transport using the photonic Aharonov–Bohm effect, Opt. Lett. **40**, 5140 (2015).

[11] M.-T. Cheng, X.-S. Ma, M.-T. Ding, Y.-Q. Luo, and G.-X. Zhao, Single-photon transport in one-dimensional coupled-resonator waveguide with local and nonlocal coupling to a nanocavity containing a two-level system, Phys. Rev. A **85**, 053840 (2012).

[12] Z. Liao, X. Zeng, S.-Y. Zhu, and M. S. Zubairy, Single-photon transport through an atomic chain coupled to a one-dimensional nanophotonic waveguide, Phys. Rev. A **92**, 023806 (2015).

[13] M.-T. Cheng, J. Xu, and G. S. Agarwal, Waveguide transport mediated by strong coupling with atoms, Phys. Rev. A **95**, 053807 (2017).

[14] G.-Z. Song, E. Munro, W. Nie, L.-C. Kwek, F.-G. Deng, and G.-L. Long, Photon transport mediated by an atomic chain trapped along a photonic crystal waveguide, Phys. Rev. A **98**, 023814 (2018).

[15] Z. Wang, L. Du, Y. Li, and Y.-X. Liu, Phase-controlled single-photon nonreciprocal transmission in a one-dimensional waveguide, Phys. Rev. A **100**, 053809 (2019).

[16] D. Mukhopadhyay and G. S. Agarwal, Transparency in a chain of disparate quantum emitters strongly coupled to a waveguide, Phys. Rev. A **101**, 063814 (2020).

[17] S. L. Feng and W. Z. Jia, Manipulating single-photon transport in a waveguide-QED structure containing two giant atoms, Phys. Rev. A **104**, 063712 (2021).

[18] Z.-R. Li, J. Dong, Y. Xu, B. Zou, and Y. Zhang, Effects of quantum interference in multi-waveguide systems bridged by Jaynes-Cummings emitters, Phys. Rev. A **105**, 053712 (2022).

[19] J.-T. Shen and S. Fan, Coherent Single Photon Transport in a One-Dimensional Waveguide Coupled with Superconducting Quantum Bits, Phys. Rev. Lett. **95**, 213001 (2005).

[20] C. Papon, X. Zhou, H. Thyrrestrup, Z. Liu, S. Stobbe, R. Schott, A. D. Wieck, A. Ludwig, P. Lodahl, and L. Midolo, Nanomechanical single-photon routing, Optica **6**, 524 (2019).

[21] T. Aoki, A. S. Parkins, D. J. Alton, C. A. Regal, B. Dayan, E. Ostby, K. J. Vahala, and H. J. Kimble, Efficient Routing of Single Photons by One Atom and a Microtoroidal Cavity, Phys. Rev. Lett. **102**, 083601 (2009).

[22] I.-C. Hoi, C. M. Wilson, G. Johansson, T. Palomaki, B. Peropadre, and P. Delsing, Demonstration of a Single-Photon Router in the Microwave Regime, Phys. Rev. Lett. **107**, 073601 (2011).

[23] H. Le Jeannic, T. Ramos, S. F. Simonsen, T. Pregnolato, Z. Liu, R. Schott, A. D. Wieck, A. Ludwig, N. Rotenberg, J. J. García-Ripoll, and P. Lodahl, Experimental Reconstruction of the Few-Photon Nonlinear Scattering Matrix from a Single Quantum Dot in a Nanophotonic Waveguide, Phys. Rev. Lett. **126**, 023603 (2021).

[24] B. Dayan, A. S. Parkins, T. Aoki, E. P. Ostby, K. J. Vahala, and H. J. Kimble, A photon turnstile dynamically regulated by one atom, Science **319**, 1062 (2008).

[25] N.-C. Kim, J.-B. Li, Z.-J. Yang, Z.-H. Hao, and Q.-Q. Wang, Switching of a single propagating plasmon by two quantum dots system, Appl. Phys. Lett. **97**, 061110 (2010).

[26] P. Bermel, A. Rodriguez, S. G. Johnson, J. D. Joannopoulos, and M. Soljacic, Single-photon all-optical switching using waveguide-cavity quantum electrodynamics, Phys. Rev. A **74**, 043818 (2006).

[27] J.-T. Shen and S. Fan, Theory of single-photon transport in a single-mode waveguide. I. Coupling to a cavity containing a two-level atom, Phys. Rev. A **79**, 023837 (2009).

[28] J.-Q. Liao, J.-F. Huang, Y.-x. Liu, L.-M. Kuang, and C. P. Sun, Quantum switch for single-photon transport in a coupled superconducting transmission-line-resonator array, Phys. Rev. A **80**, 014301 (2009).

[29] L. Zhou, Z. R. Gong, Y.-x. Liu, C. P. Sun, and F. Nori, Controllable Scattering of a Single Photon inside a One-Dimensional Resonator Waveguide, Phys. Rev. Lett. **101**, 100501 (2008).

[30] C. Wang, X.-S. Ma, and M.-T. Cheng, Giant atom-mediated single photon routing between two waveguides, Opt. Express **29**, 40116 (2021).

[31] C.-H. Yan, Y. Li, H. Yuan, and L. F. Wei, Targeted photonic routers with chiral photon-atom interactions, Phys. Rev. A **97**, 023821 (2018).

[32] D.-C. Yang, M.-T. Cheng, X.-S. Ma, J. Xu, C. Zhu, and X.-S. Huang, Phase-modulated single-photon router, Phys. Rev. A **98**, 063809 (2018).

[33] Y. T. Zhu and W. Z. Jia, Single-photon quantum router in the microwave regime utilizing double superconducting resonators with tunable coupling, Phys. Rev. A **99**, 063815 (2019).

[34] L. Zhou, L.-P. Yang, Y. Li, and C. P. Sun, Quantum Routing of Single Photons with a Cyclic Three-Level System, Phys. Rev. Lett. **111**, 103604 (2013).

[35] B. Poudyal and I. M. Mirza, Collective photon routing improvement in a dissipative quantum emitter chain strongly coupled to a chiral waveguide QED ladder, Phys. Rev. Res. **2**, 043048 (2020).

[36] X. Wang, W.-X. Yang, A.-X. Chen, L. Li, T. Shui, X. Li, and Z. Wu, Phase-modulated single-photon nonreciprocal transport and directional router in a waveguide–cavity–emitter system beyond the chiral coupling, Quantum Sci. Technol. **7**, 015025 (2022).

[37] X. Li, J. Xin, G. Li, X.-M. Lu, and L. F. Wei, Quantum routings for single photons with different frequencies, Opt. Express **29**, 8861 (2021).

[38] K. Xia, G. Lu, G. Lin, Y. Cheng, Y. Niu, S. Gong, and J. Twamley, Reversible nonmagnetic single-photon isolation using unbalanced quantum coupling, Phys. Rev. A **90**, 043802 (2014).

[39] X.-W. Xu, A.-X. Chen, Y. Li, and Y.-x. Liu, Single-photon nonreciprocal transport in one-dimensional coupled-resonator waveguides, Phys. Rev. A **95**, 063808 (2017).

[40] W.-B. Yan, W.-Y. Ni, J. Zhang, F.-Y. Zhang, and H. Fan, Tunable single-photon diode by chiral quantum physics, Phys. Rev. A **98**, 043852 (2018).

[41] L. Tang, J. Tang, W. Zhang, G. Lu, H. Zhang, Y. Zhang, K. Xia, and M. Xiao, On-chip chiral single-photon interface: Isolation and unidirectional emission, Phys. Rev. A **99**, 043833 (2019).

[42] D. Roy, Few-photon optical diode, Phys. Rev. B **81**, 155117 (2010).

[43] H. Xiao, L. Wang, L. Yuan, and X. Chen, Frequency manipulations in single-photon quantum transport under ultrastrong driving, ACS Photonics **7**, 2010 (2020).

[44] Z. Liao, H. Nha, and M. S. Zubairy, Single-photon frequency-comb generation in a one-dimensional waveguide coupled to two atomic arrays, Phys. Rev. A **93**, 033851 (2016).

[45] W. Z. Jia, Y. W. Wang, and Y.-X. Liu, Efficient single photon frequency conversion in the microwave domain using superconducting quantum circuits, Phys. Rev. A **96**, 053832 (2017).

[46] L. Du and Y. Li, Single-photon frequency conversion via a giant Λ-type atom, Phys. Rev. A **104**, 023712 (2021).

[47] L. Du, Y.-T. Chen, and Y. Li, Nonreciprocal frequency conversion with chiral Λ-type atoms, Phys. Rev. Res. **3**, 043226 (2021).

[48] D. E. Chang, A. S. Sørensen, E. A. Demler, and M. D. Lukin, A single-photon transistor using nanoscale surface plasmons, Nat. Phys. **3**, 807 (2007).

[49] M. Hafezi, D. E. Chang, V. Gritsev, E. Demler, and M. D. Lukin, Quantum transport of strongly interacting photons in a one-dimensional nonlinear waveguide, Phys. Rev. A **85**, 013822 (2012).

[50] C.-H. Yan, M. Li, X.-B. Xu, Y.-L. Zhang, H. Yuan, and C.-L. Zou, Unidirectional transmission of single photons under non-ideal chiral photon-atom interactions, Phys. Rev. A **102**, 053719 (2020).

[51] E. V. Stolyarov, Single-photon switch controlled by a qubit embedded in an engineered electromagnetic environment, Phys. Rev. A **102**, 063709 (2020).

[52] P. Kolchin, R. F. Oulton, and X. Zhang, Nonlinear Quantum Optics in a Waveguide: Distinct Single Photons Strongly Interacting at the Single Atom Level, Phys. Rev. Lett. **106**, 113601 (2011).

[53] S. Baur, D. Tiarks, G. Rempe, and S. Durr, Single-Photon Switch Based on Rydberg Blockade, Phys. Rev. Lett. **112**, 073901 (2014).

[54] C.-H. Yan, W.-Z. Jia, and L.-F. Wei, Controlling single-photon transport with three-level quantum dots in photonic crystals, Phys. Rev. A **89**, 033819 (2014).

[55] W.-B. Yan and H. Fan, Control of single-photon transport in a one-dimensional waveguide by a single photon, Phys. Rev. A **90**, 053807 (2014).

[56] C.-H. Yan and L. F. Wei, Photonic switches with ideal switching contrasts for waveguide photons, Phys. Rev. A **94**, 053816 (2016).

[57] D. Aghamalyan, J.-B. You, H.-S. Chu, C. E. Png, L. Krivitsky, and L. C. Kwek, Tunable quantum switch realized with a single Λ-level atom coupled to the microtoroidal cavity, Phys. Rev. A **100**, 053851 (2019).

[58] T. Volz1, A. Reinhard, M. Winger, A. Badolato, K. J. Hennessy, E. L. Hu, and A. Imamoglu, Ultrafast all-optical switching by single photons, Nat. Photonics **6**, 605 (2012).

[59] M. Pechal, J.-C. Besse, M. Mondal, M. Oppliger, S. Gasparinetti, and A. Wallraff, Superconducting Switch for Fast On-Chip Routing of Quantum Microwave Fields, Phys. Rev. Appl. **6**, 024009 (2016).

[60] M. Bajcsy, S. Hofferberth, V. Balic, T. Peyronel, M. Hafezi, A. S. Zibrov, V. Vuletic, and M. D. Lukin, Efficient All-Optical Switching Using Slow Light within a Hollow Fiber, Phys. Rev. Lett. **102**, 203902 (2009).

[61] R. Bose, D. Sridharan, H. Kim, G. S. Solomon, and E. Waks, Low-Photon-Number Optical Switching with a Single Quantum Dot Coupled to a Photonic Crystal Cavity, Phys. Rev. Lett. **108**, 227402 (2012).

[62] D. O'Shea, C. Junge, J. Volz, and A. Rauschenbeutel, Fiber-Optical Switch Controlled by a Single Atom, Phys. Rev. Lett. **111**, 193601 (2013).

[63] J. H. Shirley, Solution of the Schrödinger equation with a Hamiltonian periodic in time, Phys. Rev. **138**, B979 (1965).

[64] D.-W. Wang, H. Cai, R.-B. Liu, and M. O. Scully, Mesoscopic Superposition States Generated by Synthetic Spin-Orbit Interaction in Fock-State Lattices, Phys. Rev. Lett. **116**, 220502 (2016).

[65] D.-W. Wang, C. Song, W. Feng, H. Cai, D. Xu, H. Deng, H. Li, D. Zheng, X. Zhu, H. Wang, S.-Y. Zhu, and M. O. Scully, Synthesis of antisymmetric spin exchange interaction and chiral spin clusters in superconducting circuits, Nat. Phys. **15**, 382 (2019).

[66] N. Goldman and J. Dalibard, Periodically Driven Quantum Systems: Effective Hamiltonians and Engineered Gauge Fields, Phys. Rev. X **4**, 031027 (2014).

[67] D.-W. Wang, H. Cai, L. Yuan, S.-Y. Zhu, and R.-B. Liu, Topological phase transitions in superradiance lattices, Optica **2**, 712 (2015).

[68] H. Li, H. Cai, J. Xu, V. V. Yakovlev, Y. Yang, and D.-W. Wang, Quantum photonic transistor controlled by an atom in a Floquet cavity-QED system, Opt. Express **27**, 6946 (2019).

[69] S. Parkins and T. Aoki, Microtoroidal cavity QED with fiber overcoupling and strong atom-field coupling: A single-atom quantum switch for coherent light fields, Phys. Rev. A **90**, 053822 (2014).

[70] T. Yoshie, A. Scherer, J. Hendrickson, G. Khitrova, H. M. Gibbs, G. Rupper, C. Ell, O. B. Shchekin, and D. G. Deppe, Vacuum Rabi splitting with a single quantum dot in a photonic crystal nanocavity, Nature (London) **432**, 200 (2004).

[71] A. Blais, R.-S. Huang, A. Wallraff, S. M. Girvin, and R. J. Schoelkopf, Cavity quantum electrodynamics for superconducting electrical circuits: An architecture for quantum computation, Phys. Rev. A **69**, 062320 (2004).

[72] T. Hime, P. A. Reichardt, B. L. T. Plourde, T. L. Robertson, C.-E. Wu, A. V. Ustinov, and J. Clarke, Solid-State Qubits with Current-Controlled Coupling, Science **314**, 1427 (2006).

[73] M. S. Allman, J. D. Whittaker, M. Castellanos-Beltran, K. Cicak, F. da Silva, M. P. DeFeo, F. Lecocq, A. Sirois, J. D. Teufel, J. Aumentado, and R. W. Simmonds, Tunable Resonant and Nonresonant Interactions between a Phase Qubit and *LC* Resonator, Phys. Rev. Lett. **112**, 123601 (2014).

[74] Y. Chen, C. Neill, P. Roushan, N. Leung, M. Fang, R. Barends, J. Kelly, B. Campbell, Z. Chen, B. Chiaro, A. Dunsworth, E. Jeffrey, A. Megrant, J. Y. Mutus, P. J. J. O'Malley, C. M. Quintana, D. Sank, A. Vainsencher, J. Wenner, T. C. White *et al.*, Qubit Architecture with High Coherence and Fast Tunable Coupling, Phys. Rev. Lett. **113**, 220502 (2014).

[75] K. Fang, Z. Yu, and S. Fan, Realizing effective magnetic field for photons by controlling the phase of dynamic modulation, Nat. Photonics **6**, 782 (2012).

[76] K. Fang, J. Luo, A. Metelmann, M. H. Matheny, F. Marquardt, A. A. Clerk, and O. Painter, Generalized non-reciprocity in an optomechanical circuit via synthetic magnetism and reservoir engineering, Nat. Phys. **13**, 465 (2017).

[77] Y. Yin, Y. Chen, D. Sank, P. J. J. O'Malley, T. C. White, R. Barends, J. Kelly, E. Lucero, M. Mariantoni, A. Megrant, C. Neill, A. Vainsencher, J. Wenner, A. N. Korotkov, A. N. Cleland, and J. M. Martinis, Catch and Release of Microwave Photon States, Phys. Rev. Lett. **110**, 107001 (2013).

[78] Y. Maleki, C. Zhou, and M. S. Zubairy, Time-reversal-symmetry breaking and chiral quantum state manipulation in plasmonic nanorings, Phys. Rev. A **105**, 042422 (2022).

[79] P. Forn-Díaz, J. Lisenfeld, D. Marcos, J. J. García-Ripoll, E. Solano, C. J. P. M. Harmans, and J. E. Mooij, Observation of the Bloch-Siegert Shift in a Qubit-Oscillator System in the Ultrastrong Coupling Regime, Phys. Rev. Lett. **105**, 237001 (2010).

[80] T. Niemczyk, F. Deppe, H. Huebl, E. P. Menzel, F. Hocke, M. J. Schwarz, J. J. Garcia-Ripoll, D. Zueco, T. Hummer, E. Solano, A. Marx, and R. Gross, Circuit quantum electrodynamics in the ultrastrong-coupling regime, Nat. Phys. **6**, 772 (2010).

[81] J. Deng, H. Dong, C. Zhang, Y. Wu, J. Yuan, X. Zhu, F. Jin, H. Li, Z. Wang, H. Cai, C. Song, H. Wang, J. Q. You, and D.-W. Wang, Observing the quantum topology of light, Science **378**, 966 (2022).

[82] W. Liu, W. Feng, W. Ren, D.-W. Wang, and H. Wang, Synthesizing three-body interaction of spin chirality with superconducting qubits, Appl. Phys. Lett. **116**, 114001 (2020).

[83] P. Roushan, C. Neill, A. Megrant, Y. Chen, R. Babbush, R. Barends, B. Campbell, Z. Chen, B. Chiaro, A. Dunsworth, A. Fowler, E. Jeffrey, J. Kelly, E. Lucero, J. Mutus, P. J. J. O'Malley, M. Neeley, C. Quintana, D. Sank, A. Vainsencher *et al.*, Chiral ground-state currents of interacting photons in a synthetic magnetic field, Nat. Phys. **13**, 146 (2017).